Springer

Acta Mechanica Sinica

CrossMark click for updates

• RESEARCH PAPER •

Acta Mech. Sin., Vol. 38, 322038 (2022)
https://doi.org/10.1007/s10409-022-22038-x

Aerodynamic performance of the flexibility of corrugated dragonfly wings in flapping flight

Yuping Wang, Xinyi He, Guoyi He*, Qi Wang, Longsheng Chen, and Xiaochen Liu

College of Aircraft Engineering, Nanchang Hangkong University, Nanchang 330063, China

Received February 17, 2022; accepted March 7, 2022; published online June 22, 2022

At low Reynolds numbers, the variable flexibility of flapping insect wings is considered essential in improving the favorable aerodynamic forces. To further explore whether significant aerodynamic coupling exists between the microstructure and passive flexible deformation, this paper proposes three technical comparison airfoils: a corrugated wing with deformation, a symmetric flat plate wing with deformation, and a corrugated wing without deformation. Based on STAR-CCM+ software, this paper numerically solves the Navier-Stokes equations using the fluid-structure interaction method. The results show that the aerodynamic performance of the flexible corrugated wing is better than that of the rigid corrugated wing, and its lift and thrust are both improved to a certain extent, and the thrust efficiency of the flexible corrugated wing is significantly higher than that of the flexible flat plate. Although the thrust is improved, a part of the lift is lost, and as the flapping amplitude increases past 35°, the disparity gradually increases. A comparison of the flexible technical airfoils shows that the corrugated structure promotes thrust and retards lift, which is closely related to the formation and dissipation of strong vortex rings during the downstroke phase. On the premise of maintaining typical flapping without falling, dragonflies can fly with skillful efficiency by adjusting the way they flap their wings. The results of this work provide new insight into the formation and role of thrust in flapping maneuvering flight and provide a specific reference for developing new bionic flapping-wing aircraft.

Flexibility corrugated wing, Fluid-structure interaction, Unsteady aerodynamics, Forward flight

Citation: Y. Wang, X. He, G. He, Q. Wang, L. Chen, and X. Liu, Aerodynamic performance of the flexibility of corrugated dragonfly wings in flapping flight, Acta Mech. Sin. **38**, 322038 (2022), https://doi.org/10.1007/s10409-022-22038-x

1. Introduction

Insects and birds in nature can often execute incredible maneuvers, such as hovering, gliding, pitching, and rapid acceleration. Manufactured aircraft cannot match the superb flying maneuvers of insects. Over the past 30 years, researchers have continually performed experiments that simulate insects flapping their wings for efficient maneuvering flight. In previous experimental studies, Ellington et al. [1, 2] used high-speed cameras to collect parameter statistics on the movement attitudes of various small insects (dragonflies, moths, and bees) and obtained approximate kinematic parameters of insect flight, such as flapping frequency, pitch angle, and other parameters. To further estimate maneuvering speed, in subsequent years of research, Chen [3] used the high-speed camera technology to track and record multiple parts of the dragonfly's hind wing. The study found that the dragonfly's wings are not rigid parts, especially when the front edge is hinged at the wing section, and further identified two kinds of flapping modes, namely, figure-eight and double-figure-eight swing modes. Iverson et al. [4] studied the flexibility of the chord length of the flapping wings and found that flexible flapping wings can improve the thrust and movement efficiency more than rigid flapping wings. Research [5] showed that the introduction of spanwise flexibility changes the spanwise distribution of the effective angle of attack of the flapping wing. Suitable spanwise flexibility is very beneficial to

*Corresponding author. E-mail address: 70190@nchu.edu.cn (Guoyi He)

Executive Editor: Shizhao Wang

the propulsion efficiency of the flapping wing.

In the above research, wing models incorporated only simple geometric shapes. In studying the morphology and structure of the wings of dragonflies and other insects, it has been proven that the wings are a 3D corrugated structure [6]. The veins on the wings play a supporting role similar to stiffening ribs, alternating horizontally and vertically, intertwining to form a delicate polygonal structure. The fin membrane is the main aerodynamic structure, with a minimum thickness of only 0.004 mm. Rees' [7,8] flow visualization experiment found almost no difference between the corrugated wing and the flat plate and found that the incoming airflow through the corrugated airfoil is partially directed into the airfoil grooves. Kesel [9] tested a variety of cross-sectional views of the corrugated surface, incorporating different extension positions of dragonfly's wings to study, and the results showed that the lift coefficient and drag coefficient are close to those of the flat plate model when the corrugated section is not curved. The above results apply to steady-state configurations; there are few reports on the flapping motion of flapping wings. Luo et al. [10] concluded that the aerodynamic forces generated by the corrugated wing and the flat plate are approximately the same, and they explained that the corrugation length is much smaller than the flow size of the separation zone and the leading edge vortex (LEV). Du et al. [11] studied the influence of deformation and corrugated structure on aerodynamic effects during hovering, and they pointed out that the aerodynamic coupling between wing deformation and corrugation is not strong and that the corrugated structures may have more structural applications, which impact aerodynamics, but that the effect is not significant.

In recent years, Meng et al. [12] studied the effect of wing corrugation on aerodynamics and the movement of wing flapping in hovering flight. The results showed that the wing corrugations of hovering insects at typical travel amplitudes and angles of attack reduce the average lift by approximately 5%, increase the average drag by approximately 3% and barely change the location of the center of pressure. Experiments and calculations [13,14] of hovering in drosophila and hawkmoths further showed that large force coefficients could be produced when the Reynolds number exceeds 100. Luo et al. [15, 16] showed that the aerodynamic performance of a corrugated wing is better than that of a 3D flat plate at low Reynolds numbers. The presence of hind wings during gliding interferes with the evolution of the vortex structure, further affecting the aerodynamic forces. Song [17] showed that the LEV does not shed during flapping, which is the main reason for the high lift mechanism, and that the trailing edge vortex can continuously provide strong thrust during the upstroke and downstroke.

Although research has shown that flapping wings can produce high lift at low Reynolds numbers, there is no clear explanation for the high thrust and flow mechanism. The present paper numerically solves the Navier-Stokes (N-S) equations based on the previous research. Regarding the existing kinematic observation data, the interaction effects between the flexibility and the microstructure are determined by comparing the flexible corrugated wing with only the corrugated wing and the flexible corrugated wing with a flexible flat plate.

2. Numerical model and method

2.1 Microstructure of model insect wings

This paper performs the necessary simplifications based on the actual dragonfly forewing microstructure. The size changes of the wing veins and the wing membrane along the span and chord directions are ignored. The wing veins are idealized as hollow round tubes with an outer diameter of 0.18 mm and an inner diameter of 0.145 mm. The thickness of the wing membrane is 0.004 mm. The wing sections of the model wing are shown in Fig. 1.

To further explore the influence of the corrugated structure on the aerodynamic effects of flapping, a 3D flat plate with the same external figure is established. It has the same average chord length and reference area, as shown in Fig. 2.

The above two comparison models are obtained through continuous sweeping and filling in the modeling software CATIA. The geometric variables of the comparison model are given in Table 1.

Based on the reverse bionic engineering module of CATIA, the microstructure of the dragonfly wing is established at 1:1 (the polygonal structure between the wing veins and the wing membrane). The wing vein structure is replaced by a hollow round tube in the middle, and the wing membrane thickness is uniformly 0.004 mm in size. Because the wing

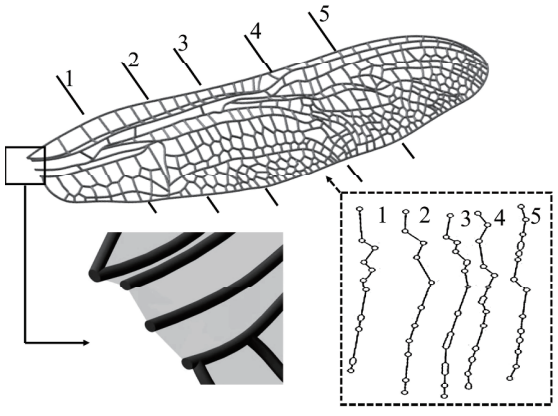

Figure 1 Corrugated forewing with corresponding details.

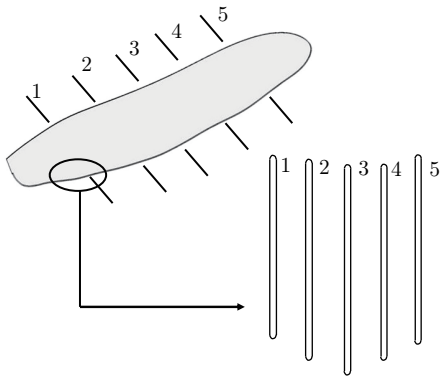

Figure 2 Three-dimensional flat plate.

Table 1 Geometric variables of the comparison models. b is the actual spanwise length of dragonfly wings. c is the chord length of dragonfly wings. d is the thickness of each section of the wings. S is the actual calculated projected area

Model	b (mm)	c (mm)	d (mm)	S (mm^2)
Corrugated structure	8	40	0.145-0.18	284.1
Flat plate	8	40	0.18	284.1

vein structure is relatively strong, it is the main load-bearing component of the dragonfly's flapping wings, and the elastic modulus and Poisson ratio are all abstracted from different experiments. The first principle ensures that the flexural stiffness (EI) is in the appropriate range. Based on Refs. [18-20], the modulus is 17 GPa, the Poisson ratio is 0.25, and the wing density is 1200 kg/m^3.

2.2 Flapping model of the wing

To clearly describe the aerodynamic effects of 3D model insect wings, we study only the simple harmonic motion of flapping around a fixed axis, where O-XYZ is the inertial coordinate system. We set the root of the branch at the center O point, and $OX'YZ'$ is the Cartesian coordinate system. This simplified flapping model can reflect the interaction between the microstructure and periodic flexible deformation, and the motion is sketched in Fig. 3.

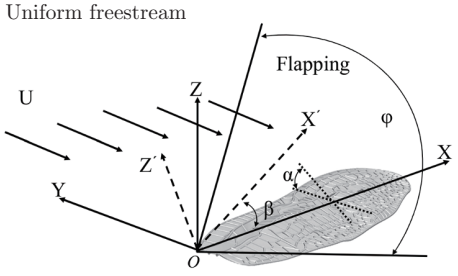

Figure 3 Sketches for the flapping motion of the dragonfly wing. U: initial incoming flow speed of 1.71 m/s; β: flapping amplitude; α: angle of attack; φ: flapping angle.

In addition, β is the angle between OX and OX', and U indicates a uniform freestream. The simple harmonic motion law of the reciprocating swing can be expressed as:

$$\varphi = \varphi_0 \sin(2\pi f t - \theta_0), \tag{1}$$

$$J = \frac{U}{4\varphi_0 b f}. \tag{2}$$

where φ is the flapping angle, J is the forward ratio, φ_0 is the flapping amplitude, θ_0 is the initial phase angle, and f is the flapping frequency, which is set at 43.4 Hz. Then, the angular velocity of the flapping is

$$\phi = \varphi' = 2\pi f \varphi_0 \cos(2\pi f t - \theta_0). \tag{3}$$

We set the left half of the fluid domain of the wing as a symmetry plane to improve computational efficiency; the direction of the incoming flow and the movement mode are given in the previous section.

2.3 Numerical methodology and setup

The wing's aerodynamic efficiency is evaluated by solving the three-dimensional incompressible Navier-Stokes equations on the overlapping grids. The formulas are as follows:

$$\nabla \cdot \boldsymbol{u} = 0, \tag{4}$$

$$\frac{\partial \boldsymbol{u}}{\partial t} + \boldsymbol{u} \cdot \nabla \boldsymbol{u} = -\nabla p + \frac{1}{Re}\nabla^2 \boldsymbol{u}, \tag{5}$$

where $\boldsymbol{u}$ is the nondimensional fluid velocity, p is the nondimensional fluid pressure, and Re denotes the Reynolds number ($Re = 1.6\times10^3$), which is defined as:

$$Re = \frac{\rho U c}{\mu}. \tag{6}$$

where ρ, U, c, and μ are taken as the freestream density, reference velocity, chord length, and dynamic viscosity coefficient, respectively ($\rho = 1.225$ kg/m^3, $U = 1.71$ m/s). When solving numerically, the components of fluid velocity and force under each time step discretely act on the wing and its surroundings (lift and drag). The expressions of the lift coefficient and drag coefficient are as follows:

$$C_\mathrm{l} = \frac{F_\mathrm{l}}{0.5\rho U^2 S}, \tag{7}$$

$$C_\mathrm{d} = \frac{F_\mathrm{d}}{0.5\rho U^2 S}. \tag{8}$$

F_l and F_d are the lift and drag, respectively. For the fluid-structure interaction, the most basic principle of conservation should be followed. The fluid area is set as the implicit unsteady-state Spalar-Allmaras turbulence model. The finite element solid stress model is adopted for the solid domain structure. The fluid region provides the external loads, and

the dragonfly wings serve as the motion boundaries required for the calculation. The interpolation and calculation are performed by decoupling the fluid domain from the solid domain partition.

$$n_{\mathrm{f}}\tau_{\mathrm{f}} = n_{\mathrm{s}}\tau_{\mathrm{s}}, \tag{9}$$

$$d_{\mathrm{q}} = d_{\mathrm{s}}, \tag{10}$$

where τ represents stress, d represents displacement, and the subscripts f and s represent fluid and solid, respectively. The first term indicates that the fluid and solid domain forces at the interface are equal, and the second indicates that the displacements are equal.

2.4 Grid independence verification

The grid is shown in Fig. 4. The calculation model uses three different grid division strategies. Under the premise of ensuring the same outflow area, the grid size is changed to verify the grid accuracy.

When the Reynolds number is 950, the initial angle of attack is 0, and the flapping amplitude is 30°, the result is as shown in Fig. 5.

Before the simulation, we considered the influence of the time grid thickness. Here, the length-to-width ratio of the calculated basin around the model is controlled at 5 to 10 times the wing chord length. Three sets of nested grids of different thicknesses are set up. The grid verification results show that when the number of nested grid elements is 8 million, 9 million, and 10 million, the errors of the lift coefficient and drag coefficient of the dragonfly's forewing are 6.5% and 4.2%, respectively. When the number of grid elements is greater than or equal to 10.08 million, the calculation result almost does not correlate with the number of elements. The fluid region grid contains 2.4 million elements, the overlapping rotation region contains 2.6 million elements, and the dragonfly wing grid contains 5.08 million elements.

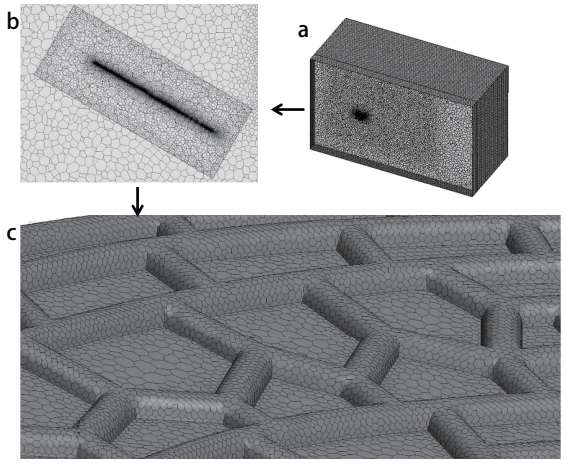

Figure 4 Schematic diagrams of the overall mesh size and local enlarged mesh size. **a** Regional mesh model of the external flow field of the dragonfly wing. **b** Local refinement of mesh cell size in overlapping areas. **c** Mesh of the corrugated forewing.

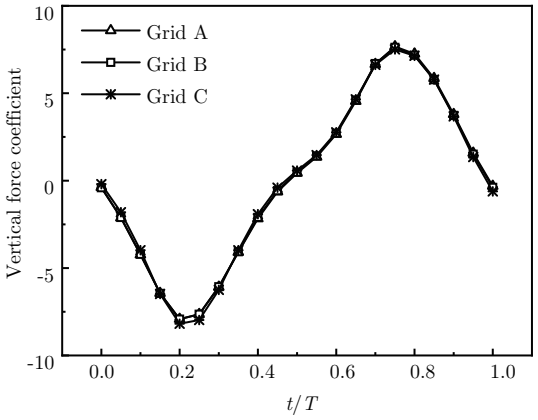

Figure 5 Comparison of independence verification results. Grid A: 8-million-element overset mesh; Grid B: 9.2-million-element overset mesh; Grid C: 10.08-million-element overset mesh.

2.5 Accuracy of the numerical method

As shown in Fig. 6, this paper selects the wing motion model of Ref. [21] to verify the accuracy of the simulation method and compare the calculation results with the literature. The comparison shows that the method adopted in this paper can be used to simulate the numerical calculation of the effective flapping of insects flying forward.

3. Results and discussion

3.1 Lift coefficient for flapping forward flight

Several different aerodynamic performance conclusions can

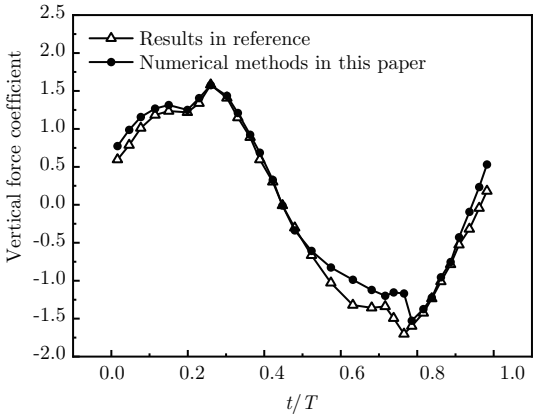

Figure 6 Results of vertical force coefficients over a cycle compared with literature reports.

be obtained by comparing the dragonfly wing microstructure and the passive flexible deformation. When the angle of attack is 0°, the flapping plane is 30° under the incoming flow of $U = 1.71$ m/s, as shown in Fig. 7.

Consider the variation in the lift coefficients of the three models when the flapping amplitude is 20°. According to Fig. 7, the forward flapping models produce two distinct lift peaks from bottom to top. The first half cycle corresponds to flapping up, and the second half cycle corresponds to flapping down. A flexible wing's time-averaged positive and negative lift is better than that of a rigid wing. During the downstroke phase, the maximum lift coefficient increases from 5.68 for the rigid corrugated wing to 7.67 for the flexible corrugated wing. Notably, the lift performance of the flexible flat plate is better than that of the flexible corrugated wing (the maximum lift coefficient is increased from 7.67 for flexible corrugated wings to 11.62 for flexible flat wings).

Figure 8 presents the aerodynamic characteristics under another flapping amplitude. We find that when the flapping amplitude changes from 20° to 35°, the results are similar to those of the previous case. A comparison of the 20° and 35° flapping wing models indicates that the latter has a much higher vertical force coefficient for the flexible dragonfly wing. This shows that during the low Reynolds number flapping process, the dragonfly can complete maneuvering flight by rapidly adjusting the flapping method (such as quickly rising).

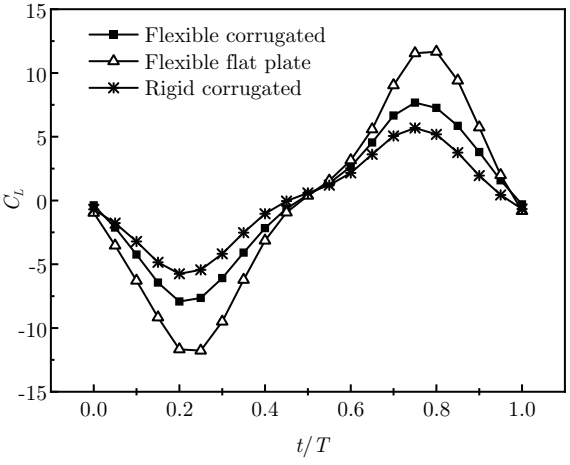

Figure 7 Lift coefficient at $\varphi_0 = 20°$. Comparison of flexible corrugated wings, flexible flat plate and rigid corrugated wings when $J = 0.4$.

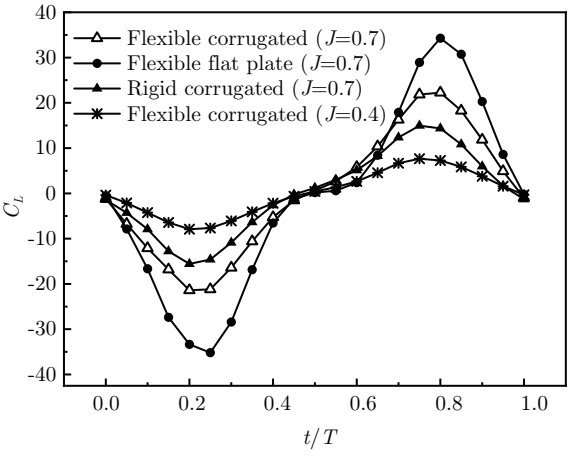

Figure 8 Lift coefficient at $\varphi_0 = 35°$. Comparison of flexible corrugated wings, flexible flat plates, and rigid folded wings with different forward ratios.

3.2 Thrust coefficient for flapping forward flight

3.2.1 Comparison of thrust between the flexible flat plate and corrugated wing

Figure 9 shows the flexibility comparison between the corrugated wing and the flat plate wing when the flapping amplitude is 20°.

First, we calculated the thrust coefficients of structures and flat plates under the same degree of flexibility, and the results are as follows. (1) From a flutter cycle, the thrust generated by the flexible corrugated wing at each moment is much greater than that of the flat plate. (2) For the flexible flat plate, the thrust coefficient exhibits periodic oscillation conclusions in both upstroke and downstroke phases; for the three-dimensional corrugated wing, a small thrust peak is generated during the upstroke phase. We hypothesize that in the process of fluttering, due to the mutual coupling of inertial force and flexibility, the wing exhibits a superposition of upward flutter and backward motion. A particular slight twist accompanies this simple harmonic and downward flutter. During the stroke phase, due to creating a new closed strong vortex ring, the thrust reaches the peak value in a cycle, explained below.

When studying flexible coupling, the microstructure reduces the maximum lift of the model wing by 52%, but the

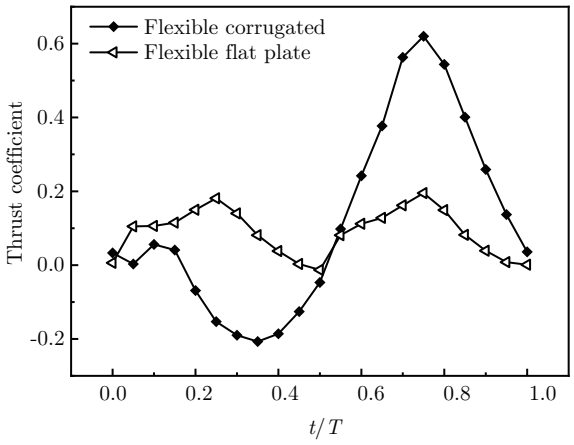

Figure 9 Comparison of the thrust between the flexible corrugated structure and flexible flat plate. The flapping angle is 20°.

thrust increases by 68%. A preliminary explanation is given. To maintain undiminished forward flapping of the flapping wing, the presence of the microstructure allows more vortices to attach to the gap. This airflow is released during the downstroke phase to form the first pair of closed strong vortex rings, providing thrust for the dragonfly to fly forward.

3.2.2 Comparison of the thrust of the rigidity and flexibility

Comparison of the rigidity and flexibility results of the corrugated wing yields fascinating conclusions.

As shown in Fig. 10, when the flapping amplitude is 20°, the motion curve fitted by the rigid wing is closer to that of the flexible corrugated forewing. Compared with the rigid wing, the thrust coefficient obtained by the adjustable wing is better.

When the flapping amplitude increases to 35°, the flexible wing fluctuates more violently. At the moment of 0.5 cycles of flapping, the dragonfly wing flaps the surrounding airflow downward from the upper pole position to obtain greater thrust.

3.3 Comparison of pressure and vorticity contours

The pressure contours and vorticity contours of the flexible plate and the flexible corrugated wing are compared in Fig. 11.

When the dragonfly flaps upward for 1/4 cycle, the maximum pressure difference of the airfoil is reached. This corresponds to the trough position of the first wave in Figs. 7 and 8. When the flapping extends for half of the period, the pressure difference between the upper and lower wing surfaces is close to 0. When reaching 3/4 cycles, corresponding to the downstroke stage of the wing, the negative pressure region

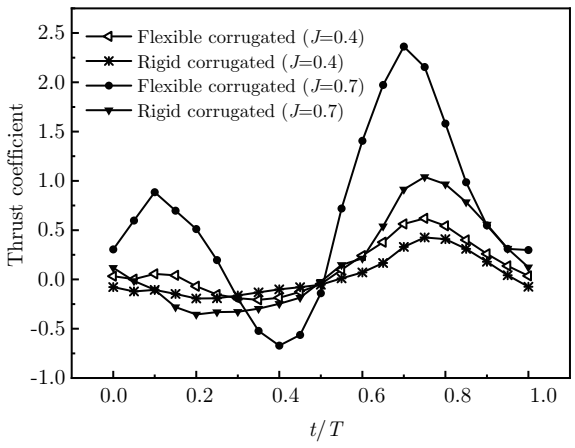

Figure 10 Rigid and flexible thrust coefficient of the corrugated wing. The different forward ratios are obtained only by changing the flapping amplitude, corresponding to $\varphi_0 = 20°$ and $\varphi_0 = 35°$.

rolls over to the top of the wing so that the opposite pressure difference reforms on the wing surface. The wing swings down until the end of the cycle. The change in the airfoil pressure difference causes the linear velocity at the wingtip to increase. The vortex under the airfoil and the trailing edge vortex roll up in the counterclockwise direction at the wingtip to form a new vortex. The closed vortex that creates the dragonfly wing's lift and thrust is enhanced. The contribution of this jet component to the thrust is better than that of the lift.

Figure 12 compares the pressure diagrams of the flexible plate and the flexible corrugated structure, allowing the following conclusions to be drawn. (1) The thin plate is a symmetrical airfoil, and the pressure difference generated at 1/4 and 3/4 times tends to spread to the wingtip and around. When fluttering occurs, more significant flexible deformation occurs. In particular, the elastic deformation reaches the maximum during the flutter, which corresponds to the upper pole (the initial moment of the flutter). (2) The contribution of the significant backpressure gradient change to the lift value is greater than the thrust value. The pressure difference of the corrugated wing is much smaller than that of the thin plate. This explains why the lift of the corrugated structure is not as strong as that of the thin plate, but the thrust has a significant gain due to the effect of the trailing edge vortex, and a different basis is given below.

Figure 13a-d shows the vorticity diagrams of the flexible corrugated wing during a flutter cycle. Due to the viscoelasticity of the flexible wings and the blocking effect of aerodynamics, we obtain a periodic solution (the second to third cycles). When the wing swings upward, only a tiny part of the leading edge vortex continues to adhere to the forewing veins, and a small number of vortices remain in the middle of the corrugated structure. More clearly visible vortices are attached to the roots of the wings. At this time, no new vortex is generated, the branch swings upward to meet the vortex formed in the previous cycle, and the lift reaches the highest value in the first half of the motion cycle.

When the dragonfly's wings continue to swing to the highest point, there is almost no new vortex above the wings, and the earliest vortex ring begins to dissipate gradually. However, when the freestream is close to the wingtip, the vortex underneath quickly converges and rolls continuously from the leading edge wingtip point to the bottom of the wing and the trailing edge wing veins. The reason is that the total vorticity varying in the span direction is very large, which induces a large downwash velocity in front of the wings, making the incoming flow almost parallel to the wing chord, so the lift at this time is minimal.

When the flapping progresses to the 3/4 cycle, a strong closed vortex ring composed of the leading-edge vortex, the wingtip vortex, and the trailing edge vortex is produced. The

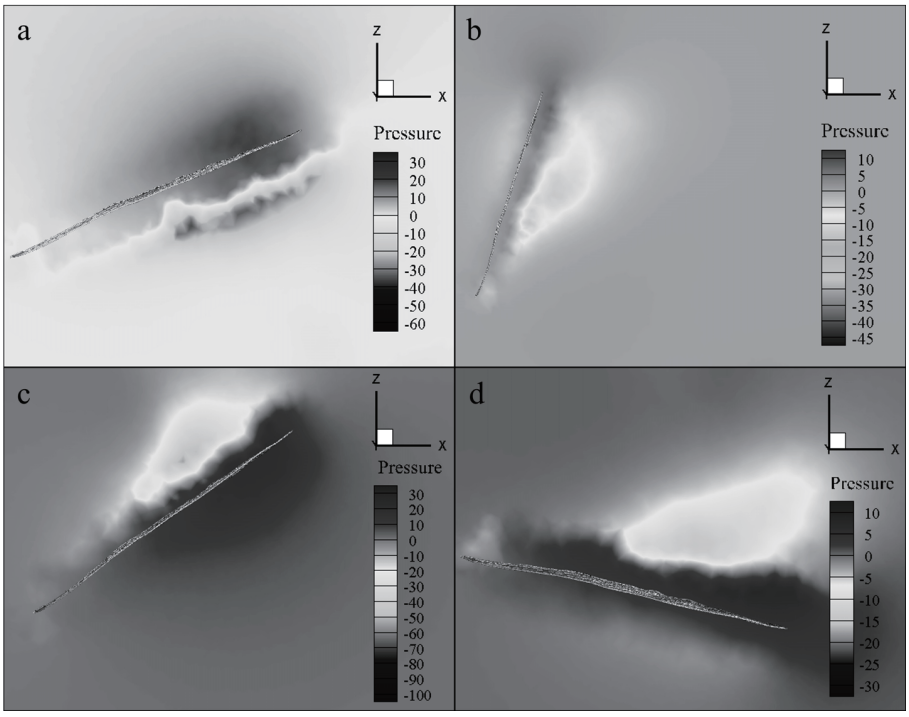

Figure 11 Pressure contours. **a** 1/4T. **b** 1/2T. **c** 3/4T. **d** 1.0T. The figure shows a stable flapping cycle of the corrugated airfoil. The sweep direction is observed from bottom to top.

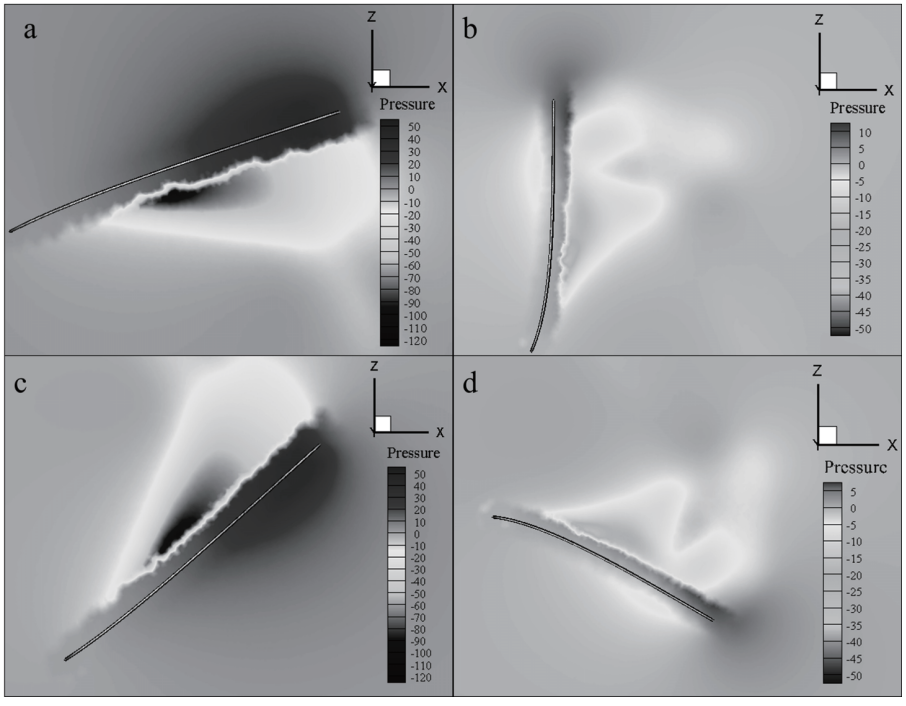

Figure 12 Pressure contours. **a** 1/4T. **b** 1/2T. **c** 3/4T. **d** 1.0T. The figure shows a stable flapping cycle of the flat plate wing. The sweep direction is observed from bottom to top.

first pair of vortices near the rear edge of the wing veins is much larger than the several pairs of diffused vortices at the rear. The most important factor is the generation and shedding of eddies on the dragonfly's flight thrust. Comparison with Fig. 9 indicates that the thrust in the downstroke stage is more than three times that in the upstroke stage and that the difference increases as the flutter amplitude increases.

Similar to the upper stroke stage, if the wings continue to

flap downward, the vortex generated before is dissipated first and is restored to the vorticity closest to the initial moment. Figure 13e-f shows the isosurface vorticity diagrams of the flexible flat plate at different times in a cycle. During the dragonfly's wing upstroke, almost no new vorticity is generated above the wing. When the wing moves to the half cycle, the leading edge detachment vortex is no longer attached to the wing surface, making the lift reach the lowest value in the rotation. In the downstroke under the same working conditions, the new vortex ring produced by the flexible flat plate is not as strong as that of the flexible corrugated wing. This phenomenon has a significant impact on the thrust. In flexibility, the time-averaged thrust coefficient increases from 1.87 for the flat plate to 2.44 for the corrugated wing, increasing by 30%.

Figure 14 compares the isosurface vorticity diagrams of a flexible wrinkled wing with a rigid wing. The trailing edge vortex never sheds during the flapping cycle, whether rigid or flexible. Note that the trailing edge vortices meet the vortices produced by the first pair as the wing flaps down and gradually weakens over time when the flapping amplitude is 20°.

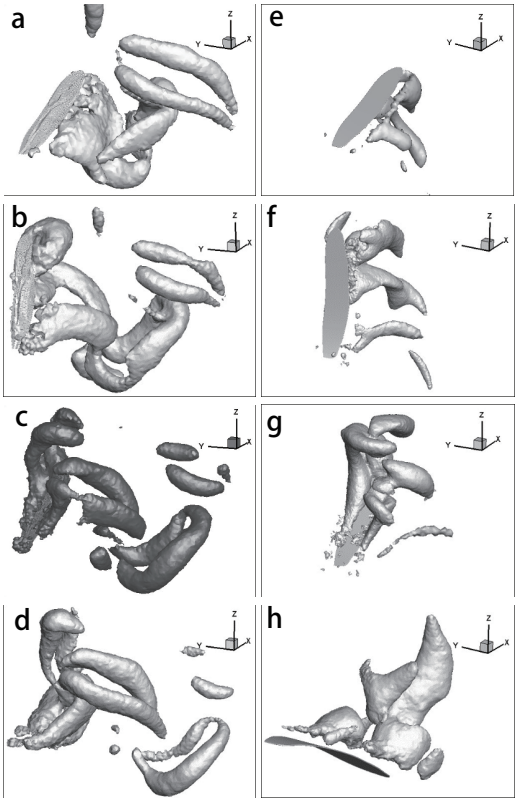

Figure 13 Isovorticity contours of the flow field within a complete flapping cycle. **a-d** show the instantaneous vorticity contours of the corrugated wing with deformation. **a** 1/4T; **b** 1/2T; **c** 3/4T; **d** 1.0T. **e-h** show the instantaneous vorticity contours of the flat plate model. **e** 1/4T; **f** 1/2T; **g** 3/4T; **h** 1.0T. The flapping direction is observed from bottom to top.

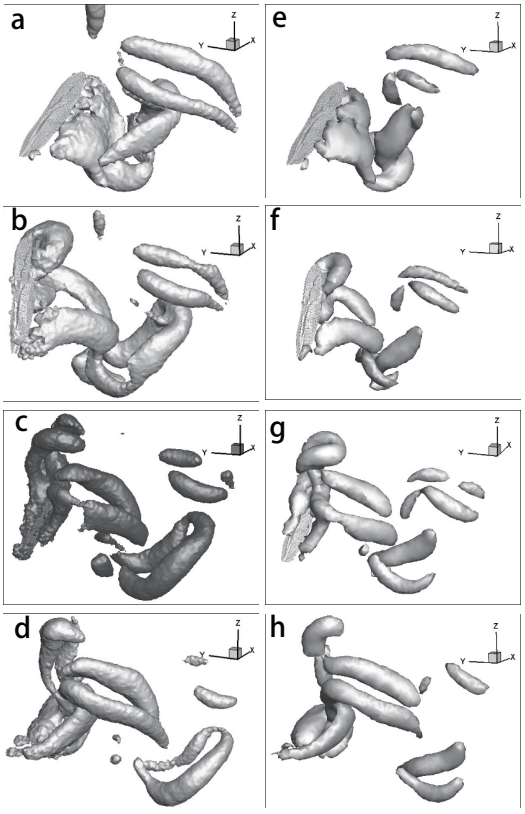

Figure 14 Isovorticity contours of the flow field within a complete flapping cycle. **a-d** show the instantaneous vorticity contours of the corrugated wing with deformation. **a** 1/4T; **b** 1/2T; **c** 3/4T; **d** 1.0T; **e-h** show the instantaneous vorticity contours of the corrugated wing without deformation. **e** 1/4T; **f** 1/2T; **g** 3/4T; **h** 1.0T. The flapping direction is observed from bottom to top.

The time-averaged thrust coefficient increases from 0.51 for the rigid corrugated wing to 2.43 for the flexible corrugated wing, which is almost an increase of 3.8 times. Therefore, we hypothesize that flexibility increases the strength of the surrounding vortices and further boosts the aerodynamic forces.

4. Conclusions

Based on the fluid-structure interaction method, we numerically solved the N-S equations and obtained the interaction relationship between the flexible deformation of the flapping wing and the microstructure. The main results are as follows.

(1) The aerodynamic efficiency focuses on observing the lift and thrust of the wing. When $\varphi_0 = 20°$, the lift and thrust of the flexible wing are more potent than that of the rigid wing, but the difference is not significant; when the flapping amplitude increases past 35°, the lift and thrust of the flexible wing are a vastly improved improvement.

(2) A flexible wing's time-averaged positive and negative lift is better than that of a rigid wing. The flexible and

rigid wings reach maximum lift values during the downstroke phase. The maximum lift coefficient increases from 5.68 for the rigid corrugated wing to 7.67 for the flexible corrugated wing. However, flexible corrugated wings do not provide as much lift as flexible flat plate wings (flexible structures have a maximum lift coefficient of 7.67, and flexible flat plates have a maximum lift coefficient of 11.62).

(3) In the forward flying state of the flapping wing, the maximum thrust coefficient of the flexible corrugated wing is 0.62, that of the flexible flat plate is 0.2, and that of the rigid corrugated wing is 0.43. The corrugated structures thus positively affect the contribution of thrust and have a retarding effect on lift.

Under the condition of maintaining routine flight without falling, the thrust of the flexible corrugated wing increases, and the attached vortex forms a strong vortex ring during the downstroke, which gradually merges with the trailing edge vortex and dissipates slowly over time. Overall, the aerodynamic performance of the flexible corrugated wing is better than that of the rigid corrugated structure, and thrust efficiency of the flexible corrugated wing is significantly higher than that of the flexible flat plate. The work can provide a specific reference for developing a new microbionic flapping vehicle.

Acknowledgements *This work was supported by the National Natural Science Foundation of China (Grant No. 11862017). The calculations were performed on Jinan Supercomputer, the National Supercomputer Center of Beijing Parallel Science and Technology.*

1 C. P. Ellington, The aerodynamics of hovering insect flight. I. The quasi-steady analysis, Phil. Trans. R. Soc. Lond. B **305**, 1 (1984).
2 C. P. Ellington, The aerodynamics of hovering insect flight. II. Morphological parameters, Phil. Trans. R. Soc. Lond. B **305**, 17 (1984).
3 Y. H. Chen, M. Skote, Y. Zhao, and W. M. Huang, Dragonfly (Sympetrum flaveolum) flight: Kinematic measurement and modelling, J. Fluids Struct. **40**, 115 (2013).
4 D. Iverson, M. Rahimpour, W. Lee, T. Kiwata, and P. Oshkai, Effect of chordwise flexibility on propulsive performance of high inertia oscillating-foils, J. Fluids Struct. **91**, 102750 (2019).
5 Y. F. Zhang, Z. Y. Ye, F. Xie, The numerical analysis of the reason for the effect of spanwise flexibility on flapping wing thrust (in Chinese), J. Eng. Mech. **30**, 419 (2013).
6 J. Fu, X. Liu, W. Shyy, and H. Qiu, Effects of flexibility and aspect ratio on the aerodynamic performance of flapping wings, Bioinspir. Biomim. **13**, 036001 (2018).
7 C. J. C. Rees, Aerodynamic properties of an insect wing section and a smooth aerofoil compared, Nature **258**, 141 (1975).
8 C. J. C. Rees, Form and function in corrugated insect wings, Nature **256**, 200 (1975).
9 A. B. Kesel, Aerodynamic characteristics of dragonfly wing sections compared with technical aerofoils, J. Exp. Biol. **203**, 3125 (2000).
10 G. Luo, and M. Sun, The effects of corrugation and wing planform on the aerodynamic force production of sweeping model insect wings, Acta Mech. Sin. **21**, 531 (2005).
11 G. Du, and M. Sun, Aerodynamic effects of corrugation and deformation in flapping wings of hovering hoverflies, J. Theor. Biol. **300**, 19 (2012).
12 X. G. Meng, L. Xu, and M. Sun, Aerodynamic effects of corrugation in flapping insect wings in hovering flight, J. Exp. Biol. **214**, 432 (2011).
13 J. H. Wu, and M. Sun, Unsteady aerodynamic forces of a flapping wing, J. Exp. Biol. **207**, 1137 (2004).
14 M. Sun, and J. Tang, Unsteady aerodynamic force generation by a model fruit fly wing in flapping motion, J. Exp. Biol. **205**, 55 (2002).
15 Y. Luo, G. Y. He, Q. Wang, H. Song, and D. H. Chen, Effect of fold structure on aerodynamic characteristics of dragonfly hind wing (in Chinese), J. Adv. Aeronaut. Eng. **10**, 355 (2019).
16 Y. Luo, G. He, H. Liu, Q. Wang, and H. Song, Aerodynamic performance of dragonfly forewing-hindwing interaction in gliding flight, IOP Conf. Ser.-Mater. Sci. Eng. **538**, 012048 (2019).
17 H. Song, G. Y. He, Q. Wang, and L. S. Chen, Numerical study on the aerodynamic performance of the rigid and corrugated forewing of dragonfly in flapping flight, IOP Conf. Ser.-Mater. Sci. Eng. **816**, 012005 (2020).
18 L. B. Meng, H. S. Ang, T. H. Xiao, Analysis of aerodynamic characteristics of flexible wing of dragonfly based on CFD/CSD method (in Chinese), J. Aerosp. Power. **29**, 2063 (2014).
19 H. Wang, L. Zeng, H. Liu, and C. Yin, Measuring wing kinematics, flight trajectory and body attitude during forward flight and turning maneuvers in dragonflies, J. Exp. Biol. **206**, 745 (2003).
20 J. S. Huang, G. Y. He, Q. Wang, Aerodynamic efficiency analysis of dragonfly flexible hind wing model, Sci. Technol. Eng. **21**, 5133 (2021).
21 K. N. Lucas, P. J. M. Thornycroft, B. J. Gemmell, S. P. Colin, J. H. Costello, and G. V. Lauder, Effects of non-uniform stiffness on the swimming performance of a passively-flexing, fish-like foil model, Bioinspir. Biomim. **10**, 056019 (2015).

柔性褶皱蜻蜓翅膀在扑翼前飞中的气动性能

王玉平, 何心怡, 何国毅, 王琦, 陈龙胜, 刘笑尘

摘要 在低雷诺数下, 拍动昆虫翅膀的可变灵活性被认为是提高有利空气动力的必要条件. 为了进一步探讨微结构与被动柔性变形之间是否存在显著的气动耦合, 本文提出了三种技术对比翼型: 变形的波纹翼、变形的对称平板翼和无变形的波纹翼. 本文基于STAR-CCM+软件, 采用流固耦合法对Navier-Stokes方程进行数值求解. 结果表明, 柔性波状翼的气动性能优于刚性波状翼, 其升力和推力均有一定程度的提高, 柔性波纹翼的推力效率明显高于柔性平板翼. 虽然推力提高了, 但也损失了一部分升力, 随着扑动幅度增加超过35°, 差距逐渐增大. 柔性技术翼型的对比表明, 褶皱结构促进推力并阻滞升力, 这与下冲程阶段强涡环的形成和消散密切相关. 蜻蜓在保持典型的拍打不坠落的前提下, 通过调整拍打翅膀的方式, 可以高效地飞行. 该工作成果为扑翼机动飞行中推力的形成和作用提供了新的认识, 为研制新型仿生扑翼飞行器提供了具体参考.